Research Article

Juan Zhang, Fuzhang Wang, Muhammad Tamoor, Muhammad Kamran, Aamir Farooq*, Sadique Rehman, Amnah S. Aljohani, Ilyas Khan, Soliman Alkhatib, and Hijaz Ahmad*

Influence of chemical reaction on MHD Newtonian fluid flow on vertical plate in porous medium in conjunction with thermal radiation

https://doi.org/10.1515/phys-2022-0028
received December 03, 2020; accepted April 04, 2022

Abstract: Our key objective in the present work is to elaborate the concept of activation energy in chemically reactive flow with the help of modeling and computation. The model investigated is fluid flow over a vertical cylinder in the porous medium with chemical reaction and radiation effect. The similarity transform converted the resulting constitutive equations and partial differential equations (PDEs) into ordinary differential equations (ODEs). The resulting non-linear momentum, heat transfer, and mass transfer coupled equations are computed with the Range–Kutta–Fehlberg method. Both assisting and non-assisting buoyant flow conditions are considered, and observed numeric solutions vary with the transport properties. Characteristics of momentum, heat, and concentration under the applied boundary conditions are analyzed. In addition, the increment in activation energy parameters boosts the Lorentz force and mass transfer rate.

Keywords: binary chemical reaction, activation energy, magnetic- and thermal-radiations, stagnation point, shooting technique

*** Corresponding author: Aamir Farooq,** Department of Mathematics, Zhejiang Normal University, Jinhua, 321004, Zhejiang, China; Department of Mathematics, Abbottabad University of Science and Technology, Abbottabad, Pakistan, e-mail: aamirf88@yahoo.com
*** Corresponding author: Hijaz Ahmad,** Section of Mathematics, International Telematic University Uninettuno, Corso Vittorio Emanuele II, 39,00186 Roma, Italy, e-mail: hijaz555@gmail.com
Juan Zhang: Guangdong ATV Academy for Performing Arts, Dongguan 523710, China
Fuzhang Wang: Nanchang Institute of Technology, Nanchang, 330044, China; School of Mathematical and Statistics, Xuzhou University of Technology, Xuzhou, 221018, China
Muhammad Tamoor: CAS Key Laboratory of Green Process and Engineering & State Key Laboratory of Biochemical Engineering, Institute of Process Engineering, Chinese Academy of Sciences, Beijing 100190, China; College of Chemical Engineering, University of Chinese Academy of Sciences, 19A Yuquan Road, Beijing 100049, China
Muhammad Kamran: Department of Mathematics, COMSATS University Islamabad, Wah Campus, 47040, Pakistan
Sadique Rehman: Department of Pure and Applied Mathematics, University of Haripur, Haripur, KPK, Pakistan
Amnah S. Aljohani: Mathematics Department, Faculty of Science, University of Tabuk, Tabuk, Saudi Arabia
Ilyas Khan: Department of Mathematics, College of Science Al-Zulfi, Majmaah University, Al-Majmaah 11952, Saudi Arabia
Soliman Alkhatib: Engineering Mathematics and Physics Department, Faculty of Engineering and Technology, Future University in Egypt, New Cairo 11845, Egypt

Nomenclature

B	magnetic field (Tesla)
C	curvature parameter (m^{-1})
C_f	skin friction coefficient (Pascal)
D	solute diffusivity ($m^2\,s$)
E	activation energy (Joules)
K	radiation parameter (–)
L, S	velocity and temperature slip length (m)
M	magnetic parameter ($W\,m^2$)
MHD	magnetohydrodynamic (–)
n	constant number (–)
Nu	Nusselt number (dimensionless number)
Pr	Prandtl number (dimensionless number)
q_m	surface mass flux ($kg\,m^{-2}\,s^{-1}$)
q_r	radiative heat flux ($kg\,s^{-3}$)
q_w	surface heat flux ($W\,m^{-2}$)
Re	Reynold's number (–)
S_c	Schmidt number (dimensionless number)
T_w	cylinder temperature (Kelvin)
T_∞	ambient temperature (Kelvin)
u, v	x, r – directions velocity ($m\,s^{-1}$)
ν	kinematic viscosity ($m^2\,s^{-1}$)

φ	concentration (volume fraction) (mol m^3)
θ	dimensionless temperature (–)
ρ	density of fluid (kg m^{-3})
η	dimensionless similarity variable (–)
σ_e	electrical conductivity
σ	reaction rate
λ	mixed convective parameter (W m^{-2} K^{-1})
c_p	specific heat (J kg^{-1} K^{-1})
ψ	stream function (–)
τ_w	cylinder temperature (Kelvin)
γ	thermal slip parameter (–)
ε	temperature difference (Kelvin)

1 Introduction

The theory of Newtonian fluid is named after Isaac Newton and has received much attention in the last several years because the non-Newtonian fluids contain fewer complex derivations and singularities. It can describe the characteristics of fluid flow precisely. Isaac was the first who had used the differential equation to postulate the relation between the shear strain rate (s^{-1}) and shear stress (mPa) for such fluids. This relationship is now known as Newton's law of viscosity (*i.e.*, shear stress (τ) = viscosity (η) × shear rate (γ)). Some η examples of Newtonian fluids are water, organic solvents, and honey. These fluid's viscosity is only dependent on temperature. Due to ideal behavior, these fluids have applications only in the theoretical studies to understand the non-Newtonian fluids.

A boundary-layer flow (BLF) is a thin-layer of viscous-fluid close to the solid surface in contact with a moving stream in which the thickness of the flow velocity varies from zero at the wall and increases up to free stream velocity at the boundary. The BLF of fluids attracted numerous researchers due to its vast applications over stretching/shrinking surfaces in different sciences and engineering fields. In the study of aerodynamical forces and their types, one can understand that the phenomena is dependent on the BLF. Few other applications of BLF are elastic sheets, tinning and strengthening of copper wires, hot rolling, fiber turning, non-stop cooling, wire drawing, paper, food processing, and expulsion of polymers. Sakiadis *et al.* was the first who examined the BLF due to its strong influence on the latest developments [1–3]. Later on, many researchers considered boundary-layer flow of Newtonian and non-Newtonian fluids. Crane *et al.* had given further directions to investigate the Sakiadis problem by utilizing the stretching boundary and evaluated the exact solutions [4]. It should be noted that many works have been done on BLF. However, we considered recently published works of BLF over a stretching surface. Nazar *et al.* had studied the unsteady flow in a rotating fluid due to suddenly stretched surface [5]. They found a smooth transition from the small-time solution to the large-time or steady-state solution. Van Gorder *et al.* had presented similar solutions for the nano BLF with the Navier boundary condition [6]. They found expected results for fluid flows at nano-scale, *i.e.*, the shear stress along the wall decreases with the increase in slip effect. Khan *et al.* had the investigated laminar fluid flow due to stretching of flat surface in a nanofluid [7]. They found that the reduced Nusselt number is a decreasing function of each dimensionless number. Ullah *et al.* had evaluated non-linear stretching of cylinder place in the porous medium [8]. They had noticed that wall shear stress magnitude is higher due to an increase in porosity. Fang *et al.* had studied the BLF over a stretching sheet with variable thickness [9]. They had observed that the stretching surface's curvature has a direct effect on the formation of the boundary layer along the wall, the velocity profiles, and the shear stress distribution in the fluid. Gireesha *et al.* had investigated numerically the effect of Copper as a nanoparticle and water with suspended particles as its base fluid on the BLF [10]. They found that momentum and thermal boundary layer are thinner due to the influence of suspended particles. Other researchers had also studied BLF [11–14] with different physical effects.

Most researchers kept up their work with the addition of assumption for different physical aspects – all this about getting close to the occurrence of real scenarios in the presence of a magnetic field, existence of magneto-hydrodynamics (MHD) flow. The projects related to engineering and technology, we mostly used MHD factor to control mass and heat transfer. In chemical engineering, experiments and numerical simulations are commonly conducted in the presence of MHD factor, see e.g. [15–18] for better understanding. The magnetic field and heat source/sink with different conditions were considered meticulously in refs. [19–21]. The presence of a magnetic field to control the different mechanisms in the material industry is important, and many researchers contributed their efforts in this direction [22–25].

The drag reduction phenomena in fluid dynamics with the surface walls are considered the slip effect. It is noticed that slip has altogether variable effects on the heat and thermal boundary layers. Slip flow due to a stretching cylinder was studied in ref. [26]. They discovered that slip significantly decreases the magnitudes of the velocities and shear stress. Hatte *et al.* had studied the analytical model for the evaluation of effective slip [27]. They discovered that liquid-infused engineered non-wetting surfaces have fluid flow with alternating no-slip and partial slip boundary conditions, resulting in decreased friction at the interface. Mukhopadhyay *et al.* explored the slip effects in the presence of MHD flow over a stretchable cylinder [28]. Numerous researchers discussed the flow problems by considering the slip conditions on the boundary [29–31].

Thermal-radiation has an important role in the surface heat transfer when the convection heat transfer coefficient is small. Its few significant applications are heating the earth by the sun, room by an open-hearth of the fireplace, circulating blood to the body, and light/heat sources in control heating systems. Due to this phenomenon, energy transfers from the source object in the form of rays. Sheikholeslami *et al.* had examined the thermal radiation effect on the MHD nanofluid flow between two horizontal rotating plates [32]. Li *et al.* had investigated the combined radiation and MHD effect on momentum and heat transfer in a vertical cylindrical annulus [33]. They observed a substantial change in temperature profile when scattering albedo reaches one. Alsagri *et al.* had founded the enhancement in the magnetic-radiations yields a decrease in the velocity field for nanoparticles [34]. Sinha *et al.* had presented the heat transfer characteristics by taking into account a steady heat supply at the wall and completely formed blood-flow through the capillary [35]. Their results revealed that the blood temperature can be controlled by regulating Joule-heating parameter. Few important studies in this physical aspect are conducted by refs. [36–39].

The heat and mass transfer in chemical reaction has important role in fluid mechanics. Due to its nature and engineering applications, it received stellar recognition. Some important applications include human transpiration, chemical catalytic reactors, nuclear reactors, electronic-equipment, gas turbines and propulsion devices, aerodynamic-extrusion of plastic sheets, filtration, refrigeration, and medicine diffusion in blood veins. The effect of the Arrhenius activation energy under the different physical conditions was discussed in [40–42]. They found that the activation energy of a chemical reaction is closely related to its rate, because molecules can only complete the reaction once they have reached the top of the activation energy barrier. Seddeek *et al.* had investigated the effect of chemical reaction on free convective flow and mass transfer over a stretching surface [43]. They noticed that an increase in the chemical parameters decreases the velocity, temperature and concentration in the boundary layer flow. Olanrewaju *et al.* analyzed the effects of thermal diffusion, including magnetic field intervention and suction/injection, on the chemical-reacting boundary-layer heat distribution and mass transfer onto a moving vertical plate [44]. Shahzed *et al.* had investigated the impacts on porous media of Casson fluid via chemical reaction, transfer of mass, and MHD flow [45].

It is obvious from the aforementioned debate that these physical effects have limited research data in a Newtonian fluid. This study has much importance to get the ideal results for understanding the behavior of the non-Newtonian fluid. The investigators plan on the collective impact of binary chemical, magnetic, and thermal radiations due to significant discussions. The model addressed here has fundamental importance. We used the numerical procedure because of the non-linearity of the mathematical model and the additional complexity factors. The numeric procedure used for the transformed dimensionless governing equations [46,47] is the Runge–Kutta–Fehlberg (RKF) method with shooting technique [48–51]. Further, surface friction and rate of heat and mass transfers are tabulated and examined for various pertinent parameters. Also, a comparison with the previous studies is mentioned for the validity of the computational process.

2 Governing equations

We will discuss the laminar BLF generated due to the non-linear stretching of the vertical cylinder (radius R). The cylinder is placed in a porous medium on the fixed surface and stretched upward. The induced magnetic field has less influence as compared to the applied magnetic field, i.e., $B = B_0 x^{(n-1)/2}$. The stretching of the cylinder sources the fluid which is placed around the cylinder. The below-given Scheme 1 shows its geometry.

$$\frac{\partial(ru_x)}{\partial x} + \frac{\partial(ru_r)}{\partial r} = 0, \tag{1}$$

$$\begin{aligned} u_x\frac{\partial u_x}{\partial x} + u_r\frac{\partial u_x}{\partial r} &= u_e\frac{\mathrm{d}u_e}{\mathrm{d}x} + \frac{\upsilon}{r}\frac{\partial}{\partial r}\left(r\frac{\partial u_x}{\partial r}\right) \\ &\quad - \left(\frac{\upsilon}{k_1} + \frac{\sigma_{(\mathrm{e})}B^2}{\rho}\right)u_x + g\beta(T - T_\infty), \end{aligned} \tag{2}$$

$$u_x\frac{\partial T}{\partial x} + u_r\frac{\partial T}{\partial r} = \frac{\alpha}{r}\frac{\partial}{\partial r}\left(r\frac{\partial T}{\partial r}\right) - \frac{1}{\rho c_p}\frac{\partial q_r}{\partial r}, \tag{3}$$

$$\begin{aligned} u_x\frac{\partial C}{\partial x} + u_r\frac{\partial C}{\partial r} &= \frac{D}{r}\frac{\partial}{\partial r}\left(r\frac{\partial C}{\partial r}\right) \\ &\quad - k_\upsilon^2(C - C_\infty)\left(\frac{T}{T_\infty}\right)^m \exp\left(\frac{E_a}{kT}\right), \end{aligned} \tag{4}$$

where u_x and u_r are the velocity components, respectively, in x and r directions; u_e is free stream velocity; $\upsilon = \frac{\mu}{\rho}$ kinematic viscosity; ρ fixed fluid density; c_p specific heat; μ coefficient of viscosity; $\sigma_{(\mathrm{e})}$ electrical conductivity; B_0 constant magnetic field; α thermal diffusivity; and q_r radiative heat flux which is calculated by Quinn Brewster [53].

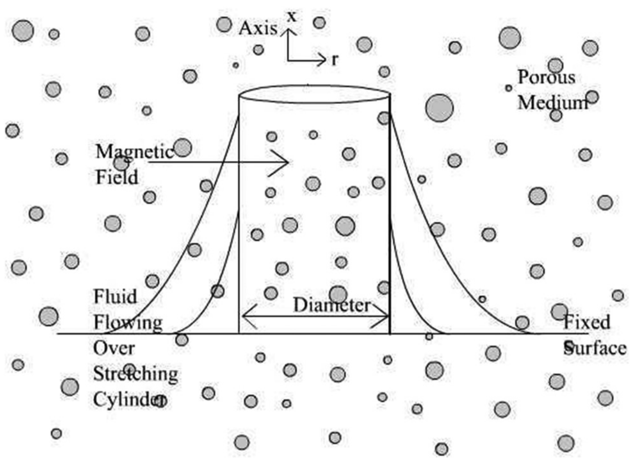

Scheme 1: Schematic representation of the geometry.

D is solute diffusivity, k is Boltzmann's constant, k_v^2 is response rate, m is fitted rate, and E_a is the activation energy. It is assumed that temperature difference inside BLF is such that T^4 may be expanded in a Taylor's series about T_∞, and removing the higher order terms we will obtain

$$q_r \approx -\frac{4\sigma^*}{3k^*}\frac{\partial T^4}{\partial r}, \tag{5}$$

and

$$T^4 \approx 4T_\infty^3 T - 3T_\infty^4, \tag{6}$$

From Eqs. (5) and (6) we get

$$q_r \approx -\frac{16\sigma^* T_\infty^3}{3k^*}\frac{\partial T}{\partial r}.$$

The appropriate Boundary Conditions (BCs) for the above problem are,

$$u_x = U + L\frac{\partial u_x}{\partial r},\; u_r = 0,\; T = T_w + S\frac{\partial T}{\partial r},\; C = C_w \quad \text{at } r = R, \tag{7-i}$$

$$u_x \to u_e,\; T \to T_\infty,\; C \to C_\infty \quad \text{as } r \to \infty, \tag{7-ii}$$

where $U = U_0 x^n$ stretching velocity; $u_e = u_0 x^n$; $T_w = T_\infty + T_0 x^{2n-1}$ surface temperature; L is the length velocity slip; C_w concentration of mass near the wall; and S is the length of the thermal slip, and $U_{(0)}$ is the reference velocity, $T_{(0)}$ is the reference temperature, $T_{(\infty)}$ is the ambient temperature, $C_{(\infty)}$ is the solute concentration.

Making use of the similarity transformations,

$$\eta = \frac{r^2 - R^2}{2R}\sqrt{\frac{U}{\upsilon x}};\; \psi = R\sqrt{U\upsilon x}f(\eta); \quad \theta(\eta) = \frac{T - T_\infty}{T_w - T_\infty};\; \varphi = \frac{C - C_\infty}{C_w - C_\infty}. \tag{8}$$

Plugging Eq. (8) in Eqs. (1–7), we will obtain the required governing equations with associated BCs. Stream function identically satisfies the continuity equation in cylindrical coordinates,

$$(1 + 2\eta C)f''' + \left(\frac{n+1}{2}\right)f f'' + 2C f'' - (M + P + n f')f' + \lambda\theta = 0, \tag{9}$$

$$\begin{aligned}&(1 + 2\eta C)[1 + \{1 + (N_r - 1)\theta\}^3\theta''] + \left[\frac{1}{2K} + \{1 + (N_r - 1)\theta\}^3\right]C\theta' \\ &+ 2(1 + 2\eta C)(N_r - 1)\{1 + (N_r - 1)\theta\}^2\theta'^2 \\ &+ \frac{\Pr}{4K}\left\{\left(\frac{n+1}{2}\right)\theta' f - (2n - 1)\theta f'\right\} = 0,\end{aligned} \tag{10}$$

$$\varphi'' + S_c f\varphi' - 2S_c\sigma\,\varphi(1 + \varepsilon\theta)^m \exp\left(\frac{-E}{1 + \varepsilon\theta}\right) = 0, \tag{11}$$

$$f' = 1 + \delta f'',\; f = 0,\; \theta = 1 + \gamma\theta',\; \varphi = 1 \quad \text{at } \eta = 0, \tag{12-i}$$

$$f' = A,\; \theta \to 0,\; \varphi \to 0 \quad \text{as } \eta \to \infty. \tag{12-ii}$$

Abovementioned pertinent parameters are curvature $C = \frac{2\chi\upsilon}{r^2 - R^2}\frac{x}{U}$, magnetic $M = \left(\frac{\sigma_{(e)}B_0^2}{\rho U_0}\right)^{\frac{1}{2}}$, porosity $P = \frac{\upsilon x}{k_1 U}$, mixed convection $\lambda = \frac{g\beta T_0}{U_0^2}$, velocity ratio $A = \frac{u_0}{U_0}$, temperature ratio $N_r = \frac{T_w}{T_\infty}$, Prandtl number $\Pr = \frac{\upsilon}{\alpha}$, velocity slip $\delta = L\left(\frac{U}{\upsilon x}\right)^{\frac{1}{2}}$, thermal slip $\gamma = S\left(\frac{U}{\upsilon x}\right)^{\frac{1}{2}}$, non-linear radiation $K = \frac{4\sigma^* T_\infty^3}{3kk^*}$, activation energy $E = \frac{E_a}{kT_\infty}$, temperature difference $\varepsilon = \frac{T_w - T_\infty}{T_\infty}$, reaction rate $\sigma = \frac{k_r^2}{c}$, and Schmidt number $S_c = \frac{\upsilon}{D}$.

The industrial interest quantities like skin friction coefficient (C_f), local Nusselt number (Nu_x), and local Sherwood number (Sh_x) are defined as,

$$C_f = \frac{2\tau_w}{\rho U^2},\quad \mathrm{Nu}_x = \frac{xq_w}{k(T_w - T_\infty)},\quad \mathrm{Sh}_x = \frac{xq_m}{D_B(C_w - C_\infty)}, \tag{13}$$

where the shear stress (τ_w), surface heat flux (q_w), and surface mass flux (q_m) are given by,

$$\tau_w = 2\mu\frac{\partial u_r}{\partial r}\bigg|_{r=R},\quad q_w = -k\frac{\partial T}{\partial r}\bigg|_{r=R},\quad q_m = -D_B\frac{\partial C}{\partial r}\bigg|_{r=R}. \tag{14}$$

Using the non-dimensional variables, we obtain

$$C_f(\mathrm{Re}_x)^{1/2} = 4f''(0),\; \mathrm{Nu}_x(\mathrm{Re}_x)^{-1/2} = -\theta'(0),\; \mathrm{Sh}_x(\mathrm{Re}_x)^{-1/2} = -\varphi'(0), \tag{15}$$

where $\mathrm{Re}_x = \frac{xU}{v}$ is the local Reynold's number.

3 Numerical technique

In order to study the flow model, the numerical scheme RKF method is used, which is reliable and efficient. Following are the mathematical steps for the RKF method:

$$\begin{aligned}
\phi_0 &= g(x_i, y_i),\\
\phi_1 &= g\left(x_i + \frac{1}{4}h, y_i + \frac{1}{4}h\phi_0\right),\\
\phi_2 &= g\left(x_i + \frac{3}{8}h, y_i + \left(\frac{3}{32}\phi_0 + \frac{9}{32}\phi_1\right)h\right),\\
\phi_3 &= g\left(x_i + \frac{12}{13}h, y_i + \left(\frac{1{,}932}{2{,}197}\phi_0 + \frac{7{,}200}{2{,}197}\phi_1 + \frac{7{,}296}{2{,}197}\phi_2\right)h\right),\\
\phi_4 &= g\left(x_i + h, y_i + \left(\frac{439}{216}\phi_0 - 8\phi_1 + \frac{3{,}860}{513}\phi_2 - \frac{545}{4{,}104}\phi_3\right)h\right),\\
\phi_5 &= g\left(x_i + \frac{1}{2}h, y_i + \left(-\frac{8}{27}\phi_0 + 2\phi_1 - \frac{3{,}544}{2{,}565}\phi_2 + \frac{1{,}859}{4{,}104}\phi_3 - \frac{11}{40}\phi_4\right)h\right),\\
y_{i+1} &= y_i + \left(\frac{25}{216}k_0 + \frac{1{,}408}{2{,}565}k_1 - \frac{2{,}197}{4{,}104}k_3 - \frac{1}{5}k_4\right)h,\\
z_{i+1} &= z_i + \left(\frac{16}{135}k_0 + \frac{6{,}656}{12{,}825}k_2 - \frac{28{,}561}{56{,}430}k_3 - \frac{9}{50}k_4 + \frac{2}{55}k_5\right)h,
\end{aligned} \tag{16}$$

where y is 4th and z is 5th order RKF. To calculate next step, we have

$$h_{\text{new}} = h_{\text{old}}\left(\frac{\varepsilon h_{\text{old}}}{2|z_{i+1} - y_{i+1}|}\right)^{\frac{1}{4}}. \tag{17}$$

We use $\Delta\eta = 0.01$ for calculation. The criteria used for convergence is the variation in the dimensional velocity, and the temperature should be less than 10^{-6} between any two consecutive iterations. The asymptotic BCs in Eq. (12) is approximated by using a value of 10 for $\eta_{\max}$ as follows:

$$\eta_{\max} = 10,\ f'(10) = 1,\ \theta(10) = 0. \tag{18}$$

4 Results and discussion

To analyze the impact of the various parameters with the fixed values of these physical parameters includes nonlinearity $n = 2.0$, curvature $C = 1.0$, magnetic $M = 1$, porosity $P = 0.3$, mixed convection $\lambda = 1.0$, temperature ratio $N_r = 0.3$, Prandtl number $\Pr = 0.5$, thermal radiation $K = 2.0$, velocity slip and thermal slip $\delta = \gamma = 0.3$, Schmidt number $S_c = 0.1$, activation energy $E_a = 0.1$, reaction rate $\sigma = 0.1$, fitted rate $m = 0.1$, and temperature difference $\varepsilon = 0.1$. Related important results are presented both in graphical and tabulated forms.

Table 1 presents a comparison between the results obtained currently and the previous results for the heat transfer rate $-\theta'(0)$.

Influence of governing parameters on velocity, temperature, and concentration profiles are depicted in Figures 1–14. Figure 1 exhibits the effect of variation in n on the fluid velocity. It is noticed that an increase in it decreases the momentum of the fluid. This behavior occurs due to the disturbance generated in the fluid particles/molecules. As a result, collisions between them enhances, which decreases the momentum.

Figure 2 depicts the influence of C on the velocity profile. It is observed that with the increase in the cylinder bending (or reduction in the area of cross-section), the momentum of fluid also enhances. It is actually due to less friction accounted for because of a decrease in the total surface area of the cylinder.

Figure 3 elucidates the effect of M on the velocity profile. It is evident that the increasing values of M reduces the fluid velocity. Also, the momentum boundary layer becomes thinner when n increase. This happens due to the resistance generated by the Lorentz force.

Figure 4 presents the effect of the variation in velocity slip on the velocity profile. As expected, the strength of the slip enhances the fluid flow, but in this case, it reduces. This change may occur due to the thermal/magnetic-radiations and chemical activity.

Table 1: Comparison of heat transfer rate in the Eq. (10) without considering n, m, C, P, δ, λ, ε, S_c, E, σ, γ, N_r

Prandtl number	Magnetic parameter	Radiation parameter	[52]	[53]	[54]	[55]	Present
1	0	0	0.9548	0.9547	0.9548	0.9547	0.9548
2				1.4714	1.4715	1.4714	1.4715
3			1.8691	1.8691	1.8691	1.8691	1.8691
5			2.5001		2.5001	2.5001	2.5001
1	1				0.8611	0.8610	0.8612
	0	1		0.5315	0.5312	0.5311	0.5313
	1				0.4505	0.4503	0.4502
2	0	0.5		1.0735		1.0734	1.0733
		1		0.8627		0.8626	0.8625
3		0.5		1.3807		1.3807	1.3807
		1		1.1214		1.1213	1.1214

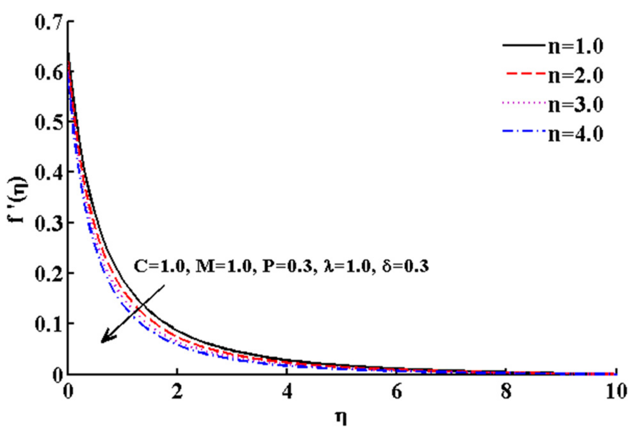

Figure 1: Effect of nonlinearly stretching parameter on fluid flow.

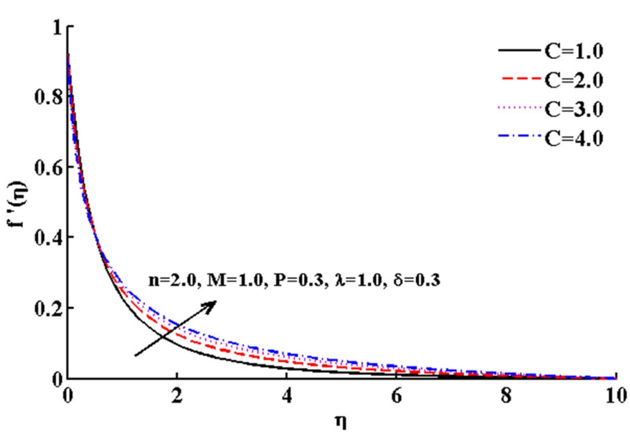

Figure 2: Effect of curvature parameter on fluid flow.

Figure 5 displays the effect of variation in A on the velocity profile, for $A > 1$ momentum and boundary layer thickness increase and *vice versa* for $A < 1$. However, for $A = 1$ no significant change is found.

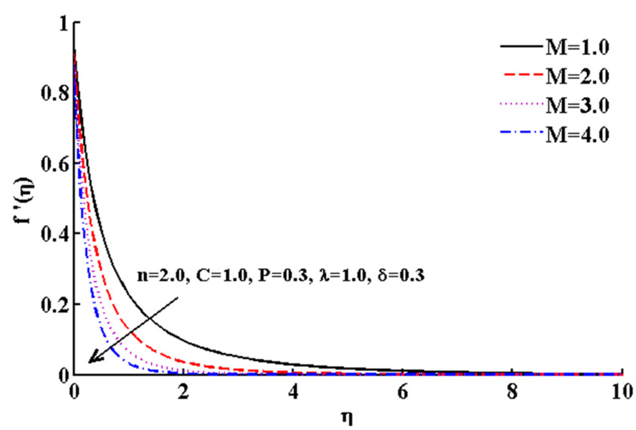

Figure 3: Effect of applied magnetic field parameter on fluid flow.

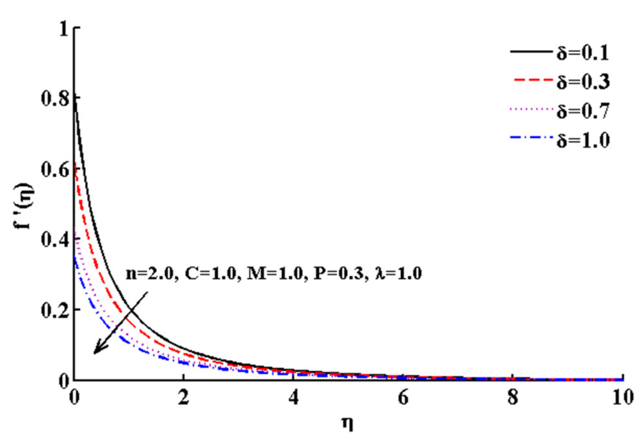

Figure 4: Effect of velocity slip parameter on fluid flow.

Figure 6 depicts the impact of C on the heat profile. By increasing curvature parameter the heat transfer reduces.

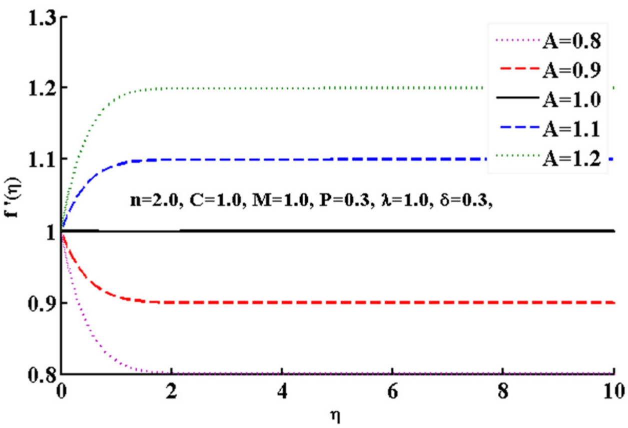

Figure 5: Effect of velocity ratio parameter on fluid flow.

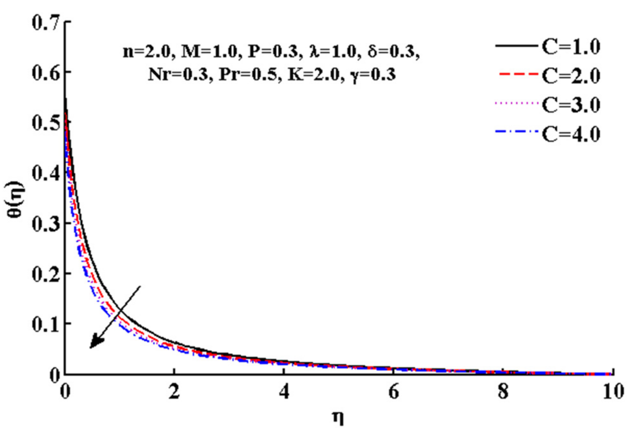

Figure 6: Effect of curvature parameter on heat transfer.

Figure 7 portrays the effect of variation in N_r on the heat profile. The thermal boundary layer becomes thicker with the increase in the temperature ratio parameter. This is because the fluid temperature is much higher than the ambient temperature for increasing values of N_r, which increases the thermal state of the fluid.

Figure 8 demonstrates the effect of K on the heat profile. As radiation parameter is representing the thermal dissipation *via* electromagnetic radiation discharge, the fluid's main energy is transformed into electromagnetic energy that enhances the internal kinetic development and collisions between the fluid molecules. Therefore, larger values of K increases the rate of heat transfer and linked thermal boundary layer. As more and more heat shift to the fluid, the temperature increases.

Figure 9 demonstrates the effect of γ on the heat profile. By increasing thermal slip parameter we noticed that the heat transfer decreases.

Figure 10 illustrates the effect of variation in S_c on the mass profile. For higher values of S_c, mass transfer reduces because the Brownian diffusion coefficient rises in such a way that it retards the mass transfer and decreases the boundary layer thickness.

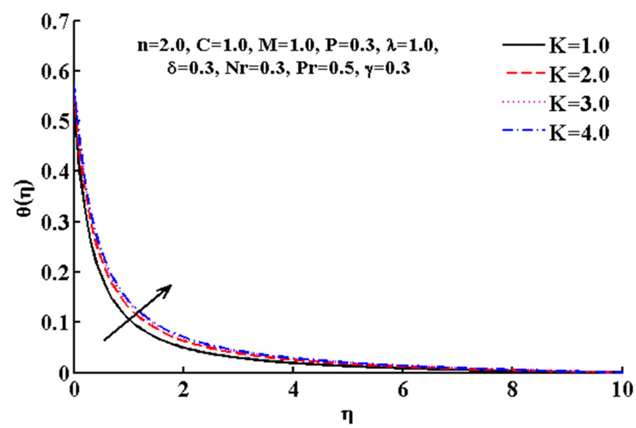

Figure 8: Effect of radiation parameter on heat transfer.

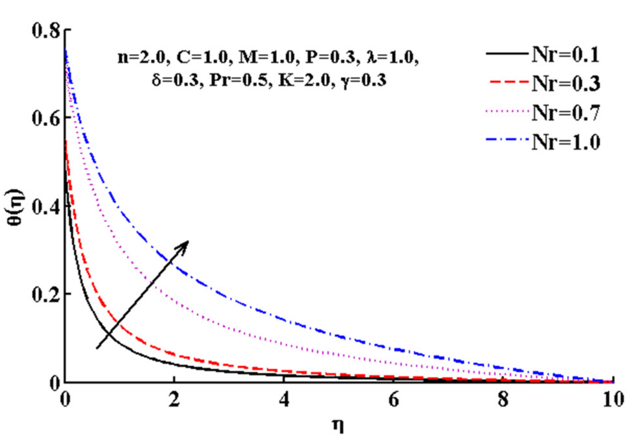

Figure 7: Effect of temperature ratio parameter on heat transfer.

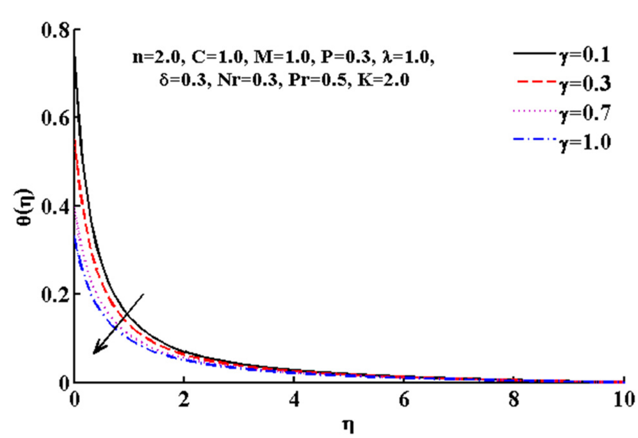

Figure 9: Effect of thermal slip parameter on heat transfer.

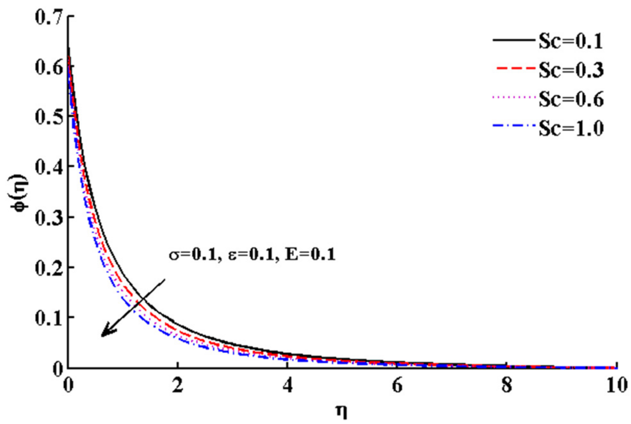

Figure 10: Effect of Schmidt number on mass transfer.

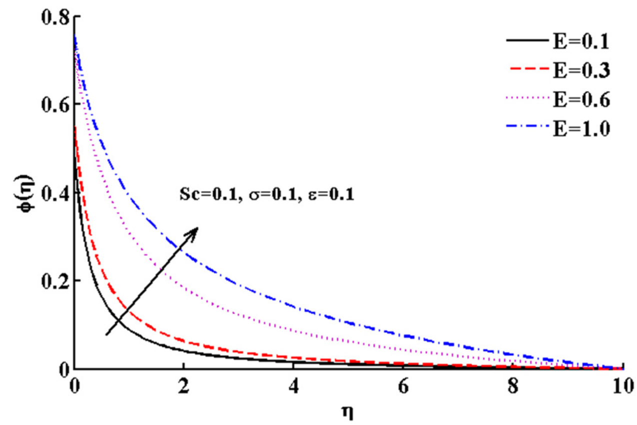

Figure 12: Effect of activation energy parameter on mass transfer.

Figure 11 displays the influence of ε on mass transfer. The mass transfer and boundary thickness both are decreasing due to increment in a temperature gradient. Our results contradict the evaluation of ref. [56]; this may be due to the stretching and shrinking effect or the radiations, and a chemical reaction occurs.

Figure 12 reveals the effect variation in E on the mass profile. From the graph, it can be seen that the concentration enhanced due to the increment in the activation energy parameter. This phenomenon is not only chemical but also physical. Therefore, to interpret the right results, more simulation and experimental results are needed by considering different kinetic parameters.

Figures 13 and 14 examine the effect variation in σ and m on the mass profile. It is clear that due to the influence of reaction rate, fitted rate increases the factor $\sigma\,(1+\varepsilon\theta)^m\varphi\,\exp\left(-\frac{E}{1+\varepsilon\theta}\right)$. An increase in the values of the reaction rate parameter implies more interaction of species concentration with the momentum boundary layer. In contrast, an increase in the fitted rate parameter illustrates the marginal rise in the concentration.

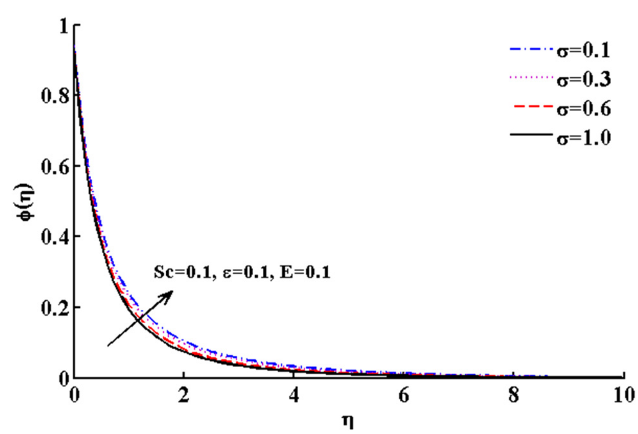

Figure 13: Effect of reaction rate parameter on mass transfer.

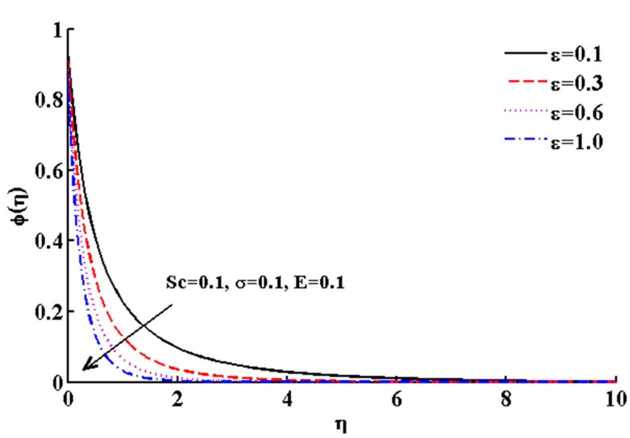

Figure 11: Effect of temperature difference parameter on mass transfer.

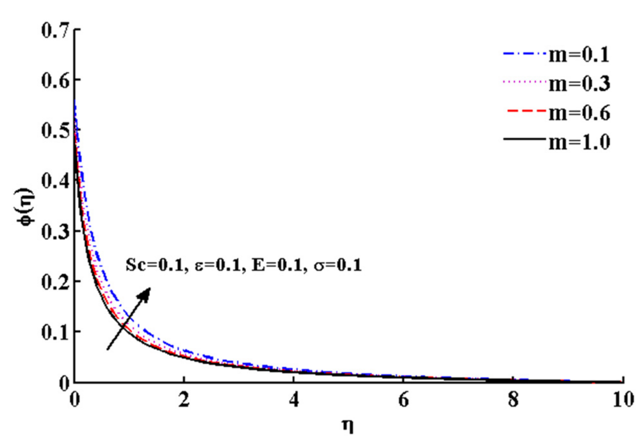

Figure 14: Effect of fitted rate constant parameter on mass transfer.

Table 2: Demonstrates the behavior of skin friction coefficient, heat, and mass transfer rates

n	C	M	P	λ	δ	N_r	Pr	K	γ	S_c	ε	E	σ	$-f''(0)$	$-\theta'(0)$	$-\theta'(0)$
1	1	1	0.3	0	0.3	0.3	0.5	2	0.3	0.1	0.1	0.1	0.1	1.17553	0.66446	
2														1.24135	0.66833	
2	2													1.36915	0.71031	
	3													1.47602	0.74113	
	1	2												1.50675		
		3												1.74290		
		1	0.1											1.28878		
			1											1.32094		
			0.3	−2										1.38645		
				2										1.10569		
				0	0.7									0.80898		
					1									0.64501		
					0.3	0.7									0.54183	
						1									0.51586	
						0.3	0.7								0.67113	
							1								0.67526	
							0.5	2							0.66833	
								3							0.65679	
								2	0.1						2.42921	
									0.7						0.86326	
									0.3	0.3						0.368195
										0.7						0.606558
										0.1	0.3					0.204370
											0.7					0.206001
											0.1	0.3				0.195759
												0.7				0.183801
												0.1	0.3			0.279629
													0.7			0.392136

In Table 2, the influence of variation in different parameters on the surface friction, heat transfer, and mass transfer rates are mentioned in detail.

5 Summary and conclusion

Two-dimensional vertical cylindrical model considered with non-linear stretching in the porous medium. Few important physical aspects included are slip, radiation, and chemical reaction. The numeric data obtained from the model is compared with previously mentioned cases. It is found that the comparison of available open literature and obtained results are in good agreement:

- An increment in the velocity slip parameter decreases the momentum of the fluid.
- The influence of the thermal slip parameter increases the heat transfer rate.
- An increase in the curvature of the cylinder makes the thermal boundary layer thinner.
- The addition of radiation energy enhances the internal kinetic development and collisions between the fluid molecules.
- Temperature gradient contains dual effects due to stretching/shrinking, radiation, and chemical reaction.
- Enhancement of reaction rate parameter generates more interaction between the species.

6 Future perspectives

Much work needed for the future perspectives,

- In the presence of radiation and chemical reaction models (specific reaction kinetics for different process).
- The geometries used in industries with 3D modeling.
- Comparison of the numerical methods and techniques for accuracy of these models are still required.
- More relevant mathematical models related to engineering applications through simulation are needed.
- Improvement needed in the numerical method algorithms.

Funding information: The authors state no funding involved.

Author contributions: All authors have accepted responsibility for the entire content of this manuscript and approved its submission.

Conflict of interest: The authors state no conflict of interest.

References

[1] Sakiadis BC. Boundary-layer behavior on continuous solid surfaces: I. Boundary-layer equations for two-dimensional and axisymmetric flow. AIChE J. 1961;7:26–8. doi: 10.1002/aic.690070108.

[2] Sakiadis BC. Boundary-layer behavior on continuous solid surfaces: II. The boundary layer on a continuous flat surface. AIChE J. 1961;7:221–5. doi: 10.1002/aic.690070211.

[3] Sakiadis BC. Boundary-layer behavior on continuous solid surfaces: III. The boundary layer on a continuous cylindrical surface. AIChE J. 1961;7:467–72. doi: 10.1002/aic.690070325.

[4] Crane LJ. Flow past a stretching plate. Z Angew Math Phys. 1970;21:645–7. doi: 10.1007/BF01587695.

[5] Nazar R, Amin N, Pop I. Unsteady boundary layer flow due to a stretching surface in a rotating fluid. Mech Res Commun. 2004;31:121–8. doi: 10.1016/j.mechrescom.2003.09.004.

[6] Van Gorder RA, Sweet E, Vajravelu K. Nano boundary layers over stretching surfaces. Commun Nonlinear Sci Numer Simul. 2010;15:1494–500. doi: 10.1016/j.cnsns.2009.06.004.

[7] Khan WA, Pop I. Boundary-layer flow of a nanofluid past a stretching sheet. Int J Heat Mass Transf. 2010;53:2477–83. doi: 10.1016/j.ijheatmasstransfer.2010.01.032.

[8] Ullah I, Alkanhal TA, Shafie S, Nisar KS, Khan I, Makinde OD. MHD slip flow of casson fluid along a nonlinear permeable stretching cylinder saturated in a porous medium with chemical reaction, viscous dissipation, and heat generation/absorption. Symmetry. 2019;11:531. doi: 10.3390/sym11040531.

[9] Fang T, Zhang J, Zhong Y. Boundary layer flow over a stretching sheet with variable thickness. Appl Math Comput. 2012;218:7241–52. doi: 10.1016/j.amc.2011.12.094.

[10] Gireesha BJ, Mahanthesh B, Gorla RSR. Suspended particle effect on nanofluid boundary layer flow past a stretching surface. J Nanofluids. 2014;3:267–77. doi: 10.1166/jon.2014.1101.

[11] Lund LA, Omar Z, Khan U, Khan I, Baleanu D, Nisar KS. Stability analysis and dual solutions of micropolar nanofluid over the inclined stretching/shrinking surface with convective boundary condition. Symmetry. 2020;12:74. doi: 10.3390/sym12010074.

[12] Lund LA, Omar Z, Khan I, Kadry S, Rho S, Mari IA, et al. Effect of viscous dissipation in heat transfer of MHD flow of micropolar fluid partial slip conditions: dual solutions and stability analysis. Energies. 2019;12:4617. doi: 10.3390/en12244617.

[13] Anwar MI, Rafique K, Misiran M, Khan I. Numerical solution of casson nanofluid flow over a non-linear inclined surface with soret and dufour effects by keller-box method. Frontiers in Physics. 2019 Oct 11;7:139. doi: 10.3389/fphy.2019.00139.

[14] Lund LA, Omar Z, Khan I, Seikh AH, Sherif E-SM, Nisar KS. Stability analysis and multiple solution of $Cu–Al_2O_3/H_2O$ nanofluid contains hybrid nanomaterials over a shrinking surface in the presence of viscous dissipation. J Mater Res Technol. 2020;9:421–32. doi: 10.1016/j.jmrt.2019.10.071.

[15] Vanita, Kumar A. Numerical study of effect of induced magnetic field on transient natural convection over a vertical cone. Alex Eng J. 2016;55:1211–23. doi: 10.1016/j.aej.2016.04.007.

[16] Xenos MA, Petropoulou EN, Siokis A, Mahabaleshwar US. Solving the nonlinear boundary layer flow equations with pressure gradient and radiation. Symmetry. 2020 May;12(5):710.

[17] Ellahi R, Alamri SZ, Basit A, Majeed A. Effects of MHD and slip on heat transfer boundary layer flow over a moving plate based on specific entropy generation. J Taibah Univ Sci. 2018;12:476–82. doi: 10.1080/16583655.2018.1483795.

[18] Dholey S. Effect of magnetic field on the unsteady boundary layer flows induced by an impulsive motion of a plane surface. Z Naturforsch A. 2020;75:343–55. doi: 10.1515/zna-2019-0334.

[19] Alarifi IM, Abokhalil AG, Osman M, Lund LA, Ayed MB, Belmabrouk H, Tlili I. MHD flow and heat transfer over vertical stretching sheet with heat sink or source effect. Symmetry. 2019 Mar;11(3):297.

[20] Waini I, Ishak A, Pop I. MHD flow and heat transfer of a hybrid nanofluid past a permeable stretching/shrinking wedge. Appl Math Mech. 2020 Mar;41(3):507–20.

[21] Zhang Y, Jiang J, Bai Y. MHD flow and heat transfer analysis of fractional Oldroyd-B nanofluid between two coaxial cylinders. Computers & Mathematics with Applications. 2019 Nov 15;78(10):3408–21.

[22] Aigbe UO, Das R, Ho WH, Srinivasu V, Maity A. A novel method for removal of Cr(VI) using polypyrrole magnetic nanocomposite in the presence of unsteady magnetic fields. Sep Purif Technol. 2018;194:377–87. doi: 10.1016/j.seppur.2017.11.057.

[23] Amiri M, Salavati-Niasari M, Akbari A. Magnetic nanocarriers: evolution of spinel ferrites for medical applications. Adv Colloid Interface Sci. 2019;265:29–44. doi: 10.1016/j.cis.2019.01.003.

[24] Tamoor M, Waqas M, Khan MI, Alsaedi A, Hayat T. Magnetohydrodynamic flow of Casson fluid over a stretching cylinder. Results Phys. 2017;7:498–502. doi: 10.1016/j.rinp.2017.01.005.

[25] Dogonchi AS, Waqas M, Seyyedi SM, Hashemi-Tilehnoee M, Ganji DD. CVFEM analysis for $Fe_3O_4–H_2O$ nanofluid in an annulus subject to thermal radiation. Int J Heat Mass Transf. 2019;132:473–83. doi: 10.1016/j.ijheatmasstransfer.2018.11.124.

[26] Wang CY, Ng C-O. Slip flow due to a stretching cylinder. Int J Non-Linear Mech. 2011;46:1191–4. doi: 10.1016/j.ijnonlinmec.2011.05.014.

[27] Hatte S, Pitchumani R. Analytical model for drag reduction on liquid-infused structured non-wetting surfaces. Soft Matter. 2021;17:1388–403. doi: 10.1039/D0SM01272F.

[28] Mukhopadhyay S. Slip effects on MHD boundary layer flow over an exponentially stretching sheet with suction/blowing and thermal radiation. Ain Shams Eng J. 2013;4:485–91. doi: 10.1016/j.asej.2012.10.007.

[29] Kumar KA, Sugunamma V, Sandeep N, Mustafa MT. Simultaneous solutions for first order and second order slips on micropolar fluid flow across a convective surface in the

presence of Lorentz force and variable heat source/sink. Sci Rep. 2019;9:14706. doi: 10.1038/s41598-019-51242-5.
[30] Ibrahim W, Shanker B. MHD boundary layer flow and heat transfer of a nanofluid past a permeable stretching sheet with velocity, thermal and solutal slip boundary conditions. Comput Fluids. 2013;75:1–10. doi: 10.1016/j.compfluid.2013.01.014.
[31] Mohamed Isa SSP, Arifin N, Farooq U. The impact of slip conditions on magneto-hydrodynamics radiating fluid beyond an exponentially extended sheet. J Phys Conf Ser. 2018;1039:012015. doi: 10.1088/1742-6596/1039/1/012015.
[32] Sheikholeslami M, domiri ganji D, Javed M, Ellahi R. Effect of thermal radiation on magneto-hydrodynamics nanofluid flow and heat transfer by means of two phase model. J Magn Magn Mater. 2015;374:36–43. doi: 10.1016/j.jmmm.2014.08.021.
[33] Li B-W, Wang W, Zhang J-K. Combined effects of magnetic field and thermal radiation on fluid flow and heat transfer of mixed convection in a vertical cylindrical annulus. J Heat Transf. 2016 Jun 1;138(6). doi: 10.1115/1.4032609.
[34] Alsagri AS, Nasir S, Gul T, Islam S, Nisar KS, Shah Z, et al. MHD thin film flow and thermal analysis of blood with CNTs nanofluid. Coatings. 2019;9(3):175. doi: 10.3390/coatings9030175.
[35] Sinha A, Shit GC. Electromagnetohydrodynamic flow of blood and heat transfer in a capillary with thermal radiation. J Magn Magn Mater. 2015;378:143–51. doi: 101016/jjmmm201411029.
[36] Xu HJ, Xing ZB, Wang FQ, Cheng ZM. Review on heat conduction, heat convection, thermal radiation and phase change heat transfer of nanofluids in porous media: fundamentals and applications. Chem Eng Sci. 2019;195:462–83.
[37] Wu H, Gui N, Yang X, Tu J, Jiang S. Numerical simulation of heat transfer in packed pebble beds: CFD-DEM coupled with particle thermal radiation. Int J Heat Mass Transf.2017;110:393–405.
[38] Rashid M, Khan MI, Hayat T, Khan MI, Alsaedi A. Entropy generation in flow of ferromagnetic liquid with non-linear radiation and slip condition. J Mol Liq. 2019;276:441–52.
[39] Daniel YS, Aziz ZA, Ismail Z, Salah F. Effects of thermal radiation, viscous and Joule heating on electrical MHD nanofluid with double stratification. Chin J Phys. 2017;55:630–51.
[40] Bestman AR. Radiative heat transfer to flow of a combustible mixture in a vertical pipe. Int J Energy Res. 1991;15:179–84. doi: 10.1002/er.4440150305.
[41] Ahmad U, Ashraf M, Khan I, Nisar K. Modeling and analysis of the impact of exothermic catalytic chemical reaction and viscous dissipation on natural convection flow driven along a curved surface. Therm Sci. 2020;24:1–11.
[42] Salawu S, Fatunmbi E, Okoya S. MHD heat and mass transport of Maxwell Arrhenius kinetic nanofluid flow over stretching surface with non-linear variable properties. Results Chem. 2021;3:100125.
[43] Seddeek M, Almushigeh A. Effects of radiation and variable viscosity on MHD free convective flow and mass transfer over a stretching sheet with chemical reaction. An Int J. 2010;5:181–97.
[44] Olanrewaju PO, Makinde OD. Effects of thermal diffusion and diffusion thermo on chemically reacting mhd boundary layer flow of heat and mass transfer past a moving vertical plate with suction/injection. Arab J Sci Eng. 2011;36:1607–19. doi: 10.1007/s13369-011-0143-8.
[45] Shehzad SA, Hayat T, Qasim M, Asghar S. Effects of mass transfer on MHD flow of Casson fluid with chemical reaction and suction. Braz J Chem Eng. 2013;30:187–95.
[46] Ali Lund L, Ching DL, Omar Z, Khan I, Nisar KS. Triple local similarity solutions of Darcy-Forchheimer magnetohydrodynamic (MHD) flow of micropolar nanofluid over an exponential shrinking surface: stability analysis. Coatings. 2019 Aug;9(8):527. doi: 10.3390/coatings9080527.
[47] Rasool G, Shafiq A, Khan I, Baleanu D, Sooppy Nisar K, Shahzadi G. Entropy generation and consequences of MHD in Darcy–Forchheimer nanofluid flow bounded by non-linearly stretching surface. Symmetry. 2020;12(4):652. doi: 10.3390/sym12040652.
[48] Hayat T, Tamoor M, Khan MI, Alsaedi A. Numerical simulation for non-linear radiative flow by convective cylinder. Results Phys. 2016;6:1031–5. doi: 10.1016/j.rinp.2016.11.026.
[49] Khan MI, Tamoor M, Hayat T, Alsaedi A. MHD boundary layer thermal slip flow by nonlinearly stretching cylinder with suction/blowing and radiation. Results Phys. 2017;7:1207–11.
[50] Rafiq M, Kamran M, Ahmed N, Mohyud-Din ST, Bashir Y, Haider SA, et al. Analytical solution for the flow of second grade fluid over a stretching sheet. AIP Adv. 2019;9:055313. doi: 10.1063/1.5093158.
[51] Shahzad A, Ali R, Kamran M, Khan SU-D, Khan SU-D, Farooq A. Axisymmetric flow with heat transfer over exponentially stretching sheet: a computational approach. Phys A Stat Mech Appl. 2020;554:124242. doi: 10.1016/j.physa.2020.124242.
[52] Magyari E, Keller B. Heat and mass transfer in the boundary layers on an exponentially stretching continuous surface. J Phys D Appl Phys. 1999;32:577–85. doi: 10.1088/0022-3727/32/5/012.
[53] Bidin B, Nazar R. Numerical solution of the boundary layer flow over an exponentially stretching sheet with thermal radiation. Eur J Sci Res. 2009;33:1450–216.
[54] Ishak A. MHD boundary layer flow due to an exponentially stretching sheet with radiation effect. Sains Malaysiana. 2011;40:391–5.
[55] Mukhopadhyay S. MHD boundary layer slip flow along a stretching cylinder. Ain Shams Eng J. 2013;4:317–24. doi: 10.1016/j.asej.2012.07.003.
[56] Eldabe N, Abu Zeid M. Thermal diffusion and diffusion thermo effects on the viscous fluid flow with heat and mass transfer through porous medium over a shrinking sheet. J Appl Math. 2013;2013:584534. doi: 10.1155/2013/584534.